激光焊熔池图像三维形态恢复算法分析

高向东，　杨永琛，　张艳喜
（广东工业大学 机电工程学院，广州　510006）

摘　要： 利用熔池图像表面的明暗变化恢复熔池表面三维形态，分析熔高和熔宽等特征与焊接质量的关系. 试验装置采用红外激光辅助光源和带有近红外窄带滤波组合系统的高速影像设备实时捕捉熔池动态图像，并根据统计学估计光源位置参数，采用基于单幅熔池灰度图像的明暗恢复形状技术（shape from shading，SFS）中的局部分析算法来恢复熔池三维表面形态，并通过中值滤波和三次样条插值对三维重建后熔池形状进行去噪和平滑处理. 结果表明，所采用的方法能有效地恢复熔池表面信息，为大功率盘形激光焊接过程中根据熔池二维图像预测焊缝成形提供了一种方法.

关键词： 大功率盘形激光焊；熔池；三维恢复
中图分类号： TG456.2　　**文献标识码：** A　　**文章编号：** 0253－360X(2013)11－0005－04

高向东

0　序　　言

大功率盘形激光焊接是当前最先进的激光焊接技术之一，具有激光功率大、光束质量优良、大深宽比和较高的激光利用率等特性[1－3]. 在大功率盘形激光焊接过程中，获取熔池形状和尺寸是实现焊接质量控制的重要前提. 焊接熔池表面形态与焊缝质量有一定的对应关系. 熟练的焊工可以通过观察熔池的形状和大小等信息感知焊接质量，通过调节焊接参数来保证焊缝成形的稳定. 熔池的三维表面恢复对于焊接自动化具有重要意义. 基于单幅图像的明暗恢复技术能够有效地恢复物体表面形态，主要包括最小值法、演化法、局部法和线性化等 4 种方法[4]. 通过建立近距离点光源混合反射模型并采用线性化方法可对熔池进行三维重建[5]. 通过反射图线性化对合成图像进行三维重建可获得良好的效果[6]. 用最小值等方法可以实现重建焊缝三维外形[7]. 局部方法的特点是只需单幅图像且三维重构速度较快，这一特点尤其适合熔池三维重构和焊接自动控制. 根据单幅熔池图像，通过估计光源倾角和偏角，建立局部分析算法数学模型，实现熔池图像的三维重建，并对不同焊接速度下熔池三维重建形态进行了分析与比较.

收稿日期： 2012－03－26
基金项目： 国家自然科学基金资助项目(51175095)；广东省自然科学基金资助项目(10251009001000001，9151009001000020)；高等学校博士学科点专项科研基金资助项目(20104420110－001)

1　试验装置

试验装置包括松下 6 关节机器人、大功率盘形激光焊接装置 TruDisk-10003、保护气体（氩气）、辅助光源、焊接工作台及图像采集系统. 图 1 为试验装置结构，焊接工艺参数见表 1. NAC 高速摄像机的拍摄速度为 5 000 幅/s，采集波段为红外光波段，图像分辨率为 500 像素 × 512 像素. 试验采用平板堆焊，试件选用尺寸为 150 mm × 100 mm × 20 mm 的 304 不锈钢.

图 1　激光焊接试验装置结构

Fig. 1　Schematic of disk laser welding experiment system

表 1　焊接工艺参数

Table 1　Welding experimental parameters

激光功率 P/kW	光斑直径 D/μm	焊接速度 v/(m·min^{-1})	氩气流量 q/(L·min^{-1})	滤波波长 λ/nm
10	480	0.6，1.5	40	960～990

2 熔池三维重构

2.1 光源位置参数估计

物体表面法线 N 可以表示为[4,8]

$$\boldsymbol{N}=(\cos\phi\sin\theta,\sin\phi\sin\theta,\cos\theta) \tag{1}$$

式中: ϕ 和 θ 为物体表面方程 $z=f(x,y)$ 上某一点 $(x,y,f(x,y))$ 处法线的倾角和偏角,反射图方程可以表达为

$$R(p,q)=\cos(\phi-\phi_s)\sin\theta\sin\theta_s+\cos\theta\cos\theta_s \tag{2}$$

式中: ϕ_s 和 θ_s 分别为光源方向的倾角和偏角; p,q 分别为物体表面某一点沿 x 和 y 方向的梯度.

光源倾角可以按照式(3)进行估计[8,9],即

$$\phi_s=\arctan\left(\frac{E\left(\dfrac{\tilde{y}_L}{\sqrt{\tilde{x}_L^2+\tilde{y}_L^2}}\right)}{E\left(\dfrac{\tilde{x}_L}{\sqrt{\tilde{x}_L^2+\tilde{y}_L^2}}\right)}\right) \tag{3}$$

式中: E 为总体均值; $\tilde{x},\tilde{y}$ 为估计的光源坐标,且

$$\begin{pmatrix}\tilde{x}_L\\ \tilde{y}_L\end{pmatrix}=(\boldsymbol{B}^{\mathrm{T}}\boldsymbol{B})^{-1}\boldsymbol{B}^{\mathrm{T}}\mathrm{d}\boldsymbol{I},\mathrm{d}\boldsymbol{I}=\begin{pmatrix}\delta I_1\\ \delta I_2\\ \vdots\\ \delta I_8\end{pmatrix},\boldsymbol{B}=\begin{pmatrix}\delta x_1 & \delta y_1\\ \delta x_2 & \delta y_2\\ \vdots & \vdots\\ \delta x_8 & \delta y_8\end{pmatrix},\delta I_i$$

为 $(\delta x_i \quad \delta y_i)$ 方向上的图像灰度变化值 $(i=1,\cdots,8)$. 其中

$$\boldsymbol{B}^{\mathrm{T}}=\begin{bmatrix}1 & \frac{\sqrt{2}}{2} & 0 & \frac{\sqrt{2}}{2} & -1 & \frac{\sqrt{2}}{2} & 0 & \frac{\sqrt{2}}{2}\\ 0 & \frac{\sqrt{2}}{2} & 1 & \frac{\sqrt{2}}{2} & 0 & \frac{\sqrt{2}}{2} & -1 & \frac{\sqrt{2}}{2}\end{bmatrix}$$

光源的偏角可以按照式(4)进行估计,即

$$\frac{E\{I_0\}}{\sqrt{E\{I_0^2\}}}=f(\theta_s) \tag{4}$$

式中: I_0 为图像上某点图像亮度; $f(\theta_s)$ 为 θ_s 的单调递减函数,且 $\theta_s\in(0,\pi/2)$.

2.2 三维重构算法

该算法的核心思想是先在光源坐标系下求得熔池表面法向量(可由倾角和偏角表示),然后通过坐标旋转将其变换到物体坐标系. 为了得到熔池表面每一点的准确尺寸,需要进行表面法向量到深度坐标值的转换.

对熔池图像而言,其表面点的亮度受到辅助激光光源、熔池表面材料性能和形状以及摄像机位置和参数等因素的影响. 传统 SFS 方法均进行了如下假设[10]: (1)光源为无限远处点光源; (2)反射模型为朗伯体反射模型; (3)成像几何关系为正交投影. 在此假设前提下,由于物体表面反射率和亮度偏移量是常量,依赖于熔池表面反射特性和背景亮度和校正等,需将其归一化处理,这样熔池图像点亮度 I_0 仅由光照方向与熔池表面法线方向的夹角 θ 的余弦决定,具体光照模型为[6,8,10]

$$R(p,q)=\cos\theta=I_0(x,y)=\frac{\cos\phi-p\cos\theta\sin\phi-q\sin\theta\sin\phi}{\sqrt{1+p^2+q^2}} \tag{5}$$

在光源坐标系下求得的物体的倾角和偏角分别为

$$\phi=\arccos\frac{E}{E_{\max}} \tag{6}$$

$$\theta=\arctan\frac{E_y\cos\theta_s-E_x\sin\theta_s}{E_x\cos\theta_s\cos\phi_s+E_y\cos\phi_s\sin\theta_s} \tag{7}$$

式中: $E_{\max}$ 为 E 最大值; E_x 和 E_y 分别表示某点在 x 方向和 y 方向上的 E 值.

由光源坐标系到物体坐标系的旋转矩阵 $\boldsymbol{R}_o$ 为

$$\boldsymbol{R}_o=\begin{bmatrix}-\cos\phi\cos\theta & \sin\phi & \sin\phi\cos\theta\\ \cos\phi\sin\theta & \cos\theta & -\sin\phi\sin\theta\\ \sin\phi & 0 & \cos\phi\end{bmatrix} \tag{8}$$

通过以上公式可以求出每个点的表面法向量,描绘出熔池的形状特点,但不能得到每一点的准确尺寸,需要进行表面法向量到深度坐标值的转换. 所有点表面法向量灰度值的归一化公式为[10]

$$z(i)_n=\frac{z_i}{\sqrt{x_i^2+y_i^2+z_i^2}}\times 255 \tag{9}$$

式中: $z(i)_n$ 为第 i 个点 (x_i,y_i,z_i) 的归一化高度.

在所有熔池图像的灰度值中找到最大值 $z_{\max}$ 和最小值 $z_{\min}$,所摄图像中熔池的最大尺寸为 $m_{\max}$,最小尺寸为 $m_{\min}$,则所有像素点对应的恢复高度值可通过计算得到,即

$$h=(z-z_{\min})(z_{\max}-z_{\min})/(z_{\max}-z_{\min})+m_{\min} \tag{10}$$

3 试验结果

3.1 光源参数估计

通过位于熔池前上方的 NAC 高速摄像机拍摄熔池图像,现选取焊接速度分别为 0.6 m/min 和 1.5 m/min 两幅熔池图像作为三维重建的试验对象,如图 2 和图 3 所示. 利用光源参数估计算法,可以得到光源的位置参数,包括光源的倾角和偏角,如表 2 所示.

3.2 熔池三维重建

利用前面所述的三维重构算法,结合光源参数估计,利用中值滤波和三次样条插值算法对重构后

的图像进行去噪滤波和平滑处理，可以得到更为平滑的熔池图像，分别如图 4 和图 5 所示.

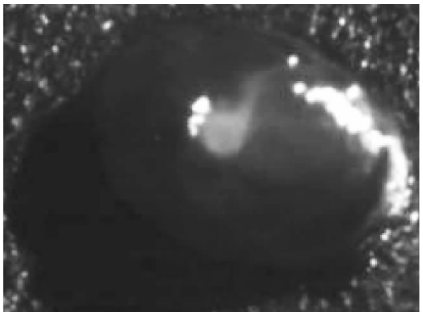

图 2　焊接速度为 0.6 m/min 的熔池原始图像

Fig. 2　Welding molten pool with welding speed 0.6 m/min

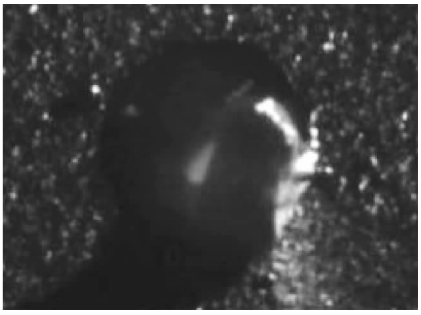

图 3　焊接速度为 1.5 m/min 的熔池原始图像

Fig. 3　Welding molten pool with welding speed 1.5 m/min

表 2　光源位置参数估计

Table 2　Estimation of illuminant direction

图像序号	图像值大小 $k_1 \times k_2$ 像素×像素	光源倾角 ϕ/rad	光源偏角 θ/rad
1	244×244	1.009 5	0.604 0
2	244×244	1.009 5	1.042 6

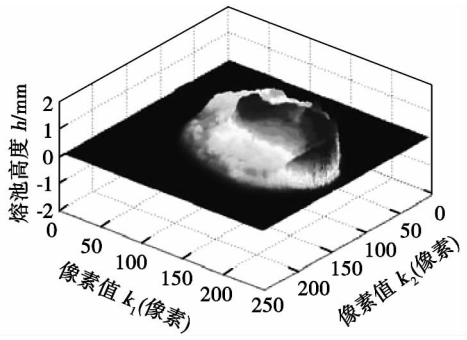

图 4　焊接速度为 0.6 m/min 的熔池三维重建结果

Fig. 4　Reconstruction shape of welding molten pool with welding speed 0.6 m/min

为了进一步观察熔池表面形态，分别提取熔池

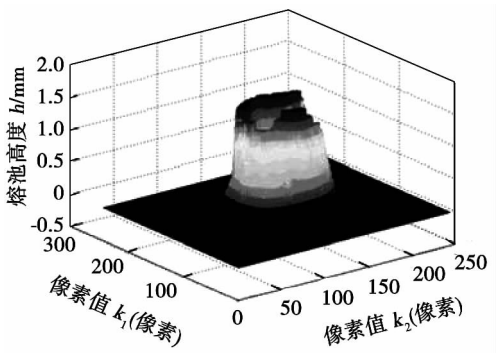

图 5　焊接速度为 1.5 m/min 的熔池三维重建结果

Fig. 5　Reconstruction shape of welding molten pool with welding speed 1.5 m/min

图像插值后第 150 行、第 200 行、第 250 行、第 300 行和第 350 行像素所对应的熔池表面形态信息，分别如图 6 和图 7 所示.

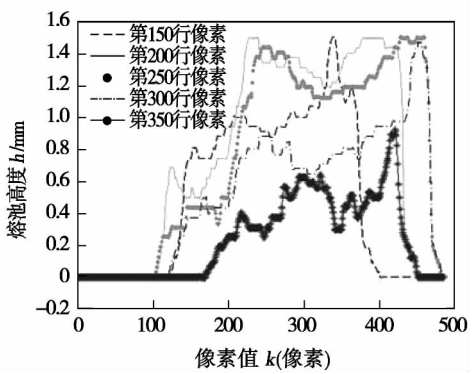

图 6　焊接速度为 0.6 m/min 的熔池表面形态分布示意图

Fig. 6　Surface of welding molten pool with speed 0.6 m/min

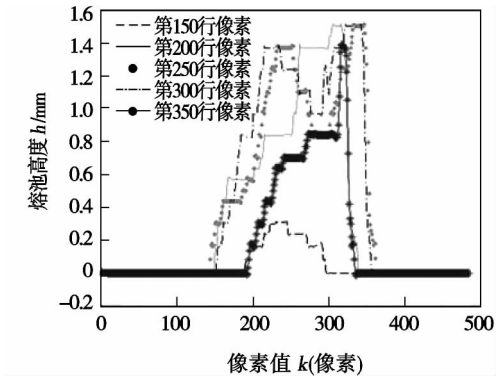

图 7　焊接速度为 1.5 m/min 的熔池的表面形态分布示意图

Fig. 7　Surface of welding molten pool with speed 1.5 m/min

从图 6 和图 7 可知，熔池整体高低形态分布趋势与实际熔池相对应，但因熔池局部存在镜面反射，

高光区域内部像素灰度相等，与周围像素形成一定的灰度差. 局部分析法是根据灰度梯度来恢复熔池高度，因此图6和图7中局部会出现较平的线段.

在图6中从第250行、300行的图线中可以看出，在200～450像素的范围内，图线先下降后上升，观察图7，同样是第250行、第300行的熔高图线中，在225～350像素的范围内呈现先下降后上升的趋势，这是由于激光焊接中熔池匙孔的存在而造成的. 另外图6中熔池较宽，而图7中熔池较窄，这与焊接速度相关. 焊接速度越慢，单位长度内焊接材料吸收的激光能量越多，从而使得熔池宽度增大.

4 结 论

(1) 对于大功率盘形激光焊接，应用辅助光源和高速像机摄取熔池图像，可提取熔池形态特征.

(2) 基于SFS原理的局部分析算法能有效地实现熔池图像的三维重建.

(3) 通过熔池表面特征点的高度分布可以获取熔池表面信息以及熔池表面高低形态变化趋势.

致谢:

感谢日本大阪大学接合科学研究所片山实验室提供的帮助!

参考文献:

[1] 高向东，吕威兴，游德勇，等. 大功率盘形激光焊接过程等离子体图像特征分析[J]. 焊接学报，2011，32(12)：5－8.
Gao Xiangdong，Lü Weixing，You Deyong，*et al*. Analysis of characteristics of plasma image during high-power disk laser welding [J]. Transactions of the China Welding Institution，2011，32(12)：5－8.

[2] Gao Xiangdong，Long Guanfu，Wang Runlin，*et al*. Analysis of characteristics of spatters during high-power disk laser welding [J]. Acta Physica Sinica，2012，61(9)：098103－1－8.

[3] Gao Xiangdong，Wang Runlin，Long Guanfu，*et al*. Study of characteristics of plume based on hue-saturation-intensity during high-power disk laser welding [J]. Acta Physica Sinica，2012，61(14)：148103－1－8.

[4] 廖 熠，赵荣椿. 从明暗恢复形状(SFS)的几类典型算法分析与评价[J]. 中国图象图形学报，2001，6(10)：953－961.
Liao Yi，Zhao Rongchun. Analysis and evaluation of several typical SFS algorithms [J]. Journal of Image and Graphics，2001，6(10)：953－961.

[5] 李来平，林 涛，陈善本. 用从明暗恢复形状方法提取焊接熔池的表面高度[J]. 焊接学报，2005，26(5)：5－8.
Li Laiping，Lin Tao，Chen Shanben. Research on shape from shading in welding pool topside height acquisition [J]. Transactions of the China Welding Institution，2005，26(5)：5－8.

[6] 赵冬斌，陈善本，吴 林. 由单目图像获得表面高度算法的分析和实现[J]. 计算机学报，2000，23(2)：147－152.
Zhao Dongbin，Chen Shanben，Wu Lin. Analysis and realization of the calculus of height from a single image [J]. Chinese Journal of Computers，2000，23(2)：147－152.

[7] 杜全营，陈善本，林 涛. 基于明暗恢复形状的焊缝外形尺寸检测[J]. 焊接学报，2004，25(5)：49－52.
Du Quanying，Chen Shanben，Lin Tao. Detection of weld shape based on shape from shading [J]. Transactions of the China Welding Institution，2004，25(5)：49－52.

[8] Zheng Qinfen，Chellappa R. Estimation of illuminant direction，albedo，and shape from shading [J]. IEEE Transactions on Pattern Analysis And Machine Intelligence，1991，13(7)：680－702.

[9] 孙林丽，李 言，郑建明. 单幅图像三维表面重建的算法研究与实现[J]. 计算机应用，2009，29(2)：433－435，443.
Sun Linli，Li Yan，Zheng Jianming. Simple 3D reconstruction method from single 2D image of object [J]. Journal of Computer Applications，2009，29(2)：433－435，443.

[10] 宋丽梅. 基于单幅实时测量图像三维形貌恢复的研究[D]. 天津：天津大学，2004.

作者简介: 高向东，男，1963年出生，教授，博士研究生导师. 主要研究方向为焊接自动控制. 发表论文150篇. Email：gaoxd666@126.com

MAIN TOPICS, ABSTRACTS & KEY WORDS

Welding deformation of top beam structure in hydraulic support by CO_2 double-wire gas shield welding based on inherent strain method FANG Chenfu, WU Wenlie, LIU Chuan, ZHONG Xulang (Provincial Key Laboratory of Advanced Welding Technology, Jiangsu University of Science and Technology, Zhenjiang 212003, China). pp 1 - 4

Abstract: The welding experiment on 30 mm thick Q690 steel plate in full-scale top beam structure of hydraulic support was carried out. The welding deformation of a relatively small structure selected from the top beam structure was firstly simulated with the thermal-elastic-plastic finite element method based on the efficient heat source model, and then the inherent strain was obtained from the small model, finally the acquired inherent strain was input into the full-scale shell element model of the hydraulic beam support structure to calculate the welding distortion deformation. The results show that, the proposed method can predict the welding deformations of large structures efficiently and accurately, the computational welding deformations of the top beam structure agree well with the experimental results; the angular distortion deformation is the main deformation of the top beam structure, which is not uniform on both sides.

Key words: hydraulic support; finite element method; inherent strain; numerical simulation; welding deformation

Analysis of 3D reconstruction algorithm of laser welding molten pool image GAO Xiangdong, YANG Yongchen, ZHANG Yanxi (School of Electromechanical Engineering, Guangdong University of Technology, Guangzhou 510006, China). pp 5 - 8

Abstract: The molten pool in high-power disk laser welding is related to the welding quality. The welding molten pool images were captured by a laser welding monitoring system. In order to reconstruct 3D shapes of the welding molten pools and further analyze the relationship between the shape features such as weld bead height, weld bead width and the welding quality, the shape from shading (SFS) technology based on single welding molten pool image was researched. 3D molten pool shapes could be recovered by the gray variations of welding molten pool image. The experimental apparatus included an auxiliary diode illuminant and a high-speed camera with near infrared filter to capture the welding molten pools in real time. The slant and tilt of illuminant source were estimated by the statistical algorithm. The 3D shape of welding molten pool surface was reconstructed by using the localization method of SFS. Also, the methods of median filter and cubic spline interpolation were applied to remove the noise and smooth the shape of molten pool. Experimental results showed that the proposed method can reconstruct the welding molten pool surface effectively. The 3D molten pool shape can be estimated by the molten pool image during high-power disk laser welding.

Key words: high-power disk laser welding; welding molten pool; 3D reconstruction

Effect of rotation frequency on microstructure and mechanical properties of refill friction spot welded Mg/Al dissimilar metals GUO Lijie[1], FENG Xiaosong[1], MIAO Yugang[2], HAN Duanfeng[2] (1. Shanghai Aerospace Equipments Manufacturer, Shanghai 200245, China; 2. College of Shipbuilding Engineering, Harbin Engineering University, Harbin 150001, China). pp 9 - 12

Abstract: AZ31 Mg alloy and 5A06 Al alloy were welded successfully with refill friction spot welding process. The shear stress of the spot joint with different tool rotation frequencies was tested. The effect of rotation frequency on the cross-section, interface layer and element distribution was analyzed. With the increase of the tool rotation speed, the shear stress of the joints increases firstly and then decreases. In particular, when the rotation speed is 2 400 r/min, the average shear stress can reach a maximum of 1.9 kN. When the rotation frequency is lower, the interface layer of Mg/Al is thiner. Due to the insufficient interface reaction, the phenomenon of incomplete fusion appears. If the rotation frequency is higher, the interface layer of Mg/Al is thicker (about 5 μm). The interface bonding is very good.

Key words: refill friction spot welding; dissimilar metals; rotation frequency; interface layer; mechanical properties

Formability and microstructure of magnesium alloy welded by A-TIG under magnetic field SU Yunhai[1,2], LIN Jinliang[1], JIANG Huanwen[1], LIU Zhengjun[1] (1. Liaoning Provincal Key Laboratory of Advaced Welding Technology and Automation, Shenyang Unviersity of Technology, Shenyang 110870, China; 2. Chinese National Engineering Research Center, Liaoning Julong Financial Equipment Corp., Anshan 114041, China). pp 13 - 16

Abstract: The AZ31B magnesium alloy plates of 5 mm in thickness were welded by A-TIG welding under longitudinal magnetic field. The mixed oxides were used as activating fluxes. The form factor, microstructure and mechanical properties of welded joint at different magnetic field parameters were tested. The effects of magnetic field parameters on A-TIG welding process of magnesium alloy were also investigated. The results show that the formability and microstructure of magnesium alloy welded joint can be improved due to the magnetic field. When the magnetic frequency is 10Hz and the magnetic current is 2 A, the form factor and properties of welded joint are tested, the form factor is 2.304 and the hardness is 980.98 MPa. The flow of molten pool will be changed by the activating fluxes and electromagnetic (which forming by magnetic field). The liquid metal in molten pool will move from all around to center, which makes the weld be deeper, refines the microstructure and improves the properties